Supplemental Information: Cooperative spin transition of monodispersed FeN_3 sites within graphene induced by CO adsorption

Qin-Kun Li[1], Xiao-Fei Li[2], Guozhen Zhang[1,*], Jun Jiang[1,*]

October 1, 2018

[1]Hefei National Laboratory for Physical Sciences at the Microscale, iChEM (Collaborative Innovation Center of Chemistry for Energy Materials), School of Chemistry and Materials Science, University of Science and Technology of China, Hefei, Anhui 230026, China,

[2]School of Optoelectronic Science and Engineering, University of Electronic Science and Technology of China, Chengdu, Sichuan, 610054, China,

Correspondence and requests for materials should be addressed to G.Z. (guozhen@ustc.edu.cn), J.J. (jiangj1@ustc.edu.cn).

Computational Details

Spin-polarized Density functional theory (DFT) simulations were implemented in Vienna Ab-initio Simulation Package (VASP)[1, 2] with generalized gradient approximation (GGA) of Perdew-Burke-Ernzerhof (PBE) exchange correlation functional.[3] Strong Coulomb interactions of 3d electron of transition metal were described with DFT+U approach[4, 5], in which Hubbard U and on-site exchange constant J were 4 and 1 eV, respectively.[6] These values were previously reported to demonstrate accurately the spin state in transition metal chemistry.[7, 8] The interaction between core electrons and valence electrons was represented by projected augmented wave (PAW) method[9, 10] and cutoff energy for the plane wave basis set is 500 eV. The van der Waals interaction was considered by DFT-D2 correction of Grimme scheme.[11] The force and energy convergence criterion were set to 0.01 eV/Å and 10^{-6} eV, respectively. Two single Fe atoms were anchored onto 8×8 graphene monolayer separated by a vacuum layer of 18 Å and k-point sampling of first Brillioun zone was used with a $3\times3\times1$ Γ-centered grid for geometry optimizations. [12]

More specifically, in our calculation, to find the magnetic ordering of Fe atoms in magnetic ground state during the stepwise CO and O_2 adsorption, we have considered NM, FM, AFM ordering with different initial value on Fe atoms. We have tried as many initial vaules of spin moment as possible to find the lowest energy. Then we compare the corresponding total energies of these magnetic states and the lowest one is deemed as the magnetic ground state. Such calculation is widely adopted by theoretical community to explore the most stable magnetic ordering and related magnetic properties in ferromagnetism and ferroelectricity fields, which provides reasonable agreement with experimental findings.[13, 14, 15, 16, 17, 18]

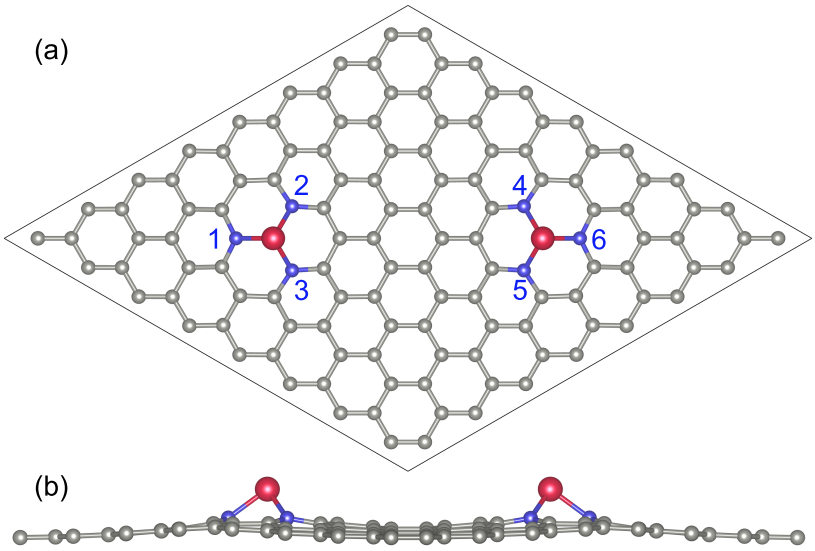

FIG. S1: Top view (a) and side view (b) of the optimized structure of FeN_3-FeN_3. The labeled numbers differentiate the N atoms for the purpose of comparing the changes of Fe-N bond length.

Table S1: The geometrical and electronic transformation of FeN_3-FeN_3 upon various CO adsorption concentration

CO Molecules [a]	Energy[b] (eV)	Spin Moment (μ_B)			Fe-N Bond Length[f] (Å)	Fe-C (CO) Bond Length[g] (Å)
		Total[c]	Left[d]	Right[e]		
0	0.00	8.47	3.41	3.41	1.955,1.965,1.965,1.964,1.964,1.954	1.143
1	-1.86	-1.12	2.81	-3.39	1.995,2.053,2.053,1.957,1.945,1.957	1.174
2	-1.70	0.00	2.89	-2.89	1.983,2.034,2.034,2.035,2.035,1.983	1.171,1.171
3	-1.23	4.36	1.03	2.96	1.977,2.035,1.978,2.018,2.018,1.974	1.169,1.168,1.168
4	-1.20	0.00	1.02	-1.03	1.977,2.034,1.977,2.035,1.977,1.977	1.168,1.168,1.168,1.168

[a] n (n= 0,1,2,3,4) CO molecules is adsorbed onto the Fe active sites orderly, n = 0 represents the bare FeN_3-FeN_3;
[b] Taking the energy of FeN_3-FeN_3 as reference energy, the energy change (ΔE) of each CO adsorption, $\Delta E = E_{(n+1)CO@FeN_3-FeN_3} - E_{CO} - E_{nCO@FeN_3-FeN_3}$;
[c] Total spin moment of FeN_3-FeN_3 framework shown in the FIG. S1;
[d] Spin moment of the left Fe atom shown in the FIG. S1;
[e] Spin moment of the right Fe atom shown in the FIG. S1;
[f] The Fe-N_m bond length in the FeN_3-FeN_3 active site ordered by increasing m values (m = 1,2,3,4,5,6) shown in the FIG. S1;
[g] The Fe-C (CO) bond length is arranged in the sequence of CO adsorption;

Table S2: The geometrical and electronic transformation of FeN_3-FeN_3 upon various O_2 adsorption concentration

O_2 Molecules	Energy (eV)	Spin Moment (μ_B)			Fe-N Bond Length (Å)
		Total	Left	Right	
0	0.00	8.47	3.41	3.41	1.955,1.965,1.965,1.964,1.964,1.954
1	-2.77	1.09	-2.74	3.39	1.955,1.954,2.035,1.950,1.957,1.951
2	-2.59	0.00	2.76	-2.76	1.949,2.025,1.949,2.025,1.949,1.949

Table S3: the calculated spin moment of adjacent Fe atoms by HSE06 functional

CO molecules	Spin Moment (μ_B)		
	Total	Left	Right
0	8.47	3.40	3.40
1	2.95	-1.02	3.38
2	0.01	2.95	-2.95
3	-2.34	1.06	-3.05
4	0.00	1.06	-1.06

Compared to PBE+U results, there exists some inconsistency of spin moment on individual Fe atoms in the cases of 1 CO and 3 CO adsorption. Since HSE06 method is quite time-consuming in periodic DFT calculations, an exhaustive search of all possible spin configurations for these two would be computationally prohibitive. Nevertheless, the finished HSE06 results clearly show cooperative communication between two adjacent Fe sites as reflected by continuous cooperative spin transitions of two neighboring Fe sites upon CO adsorption, which is in line with PBE +U results. In addition, we have compared the FM and AFM spin alignment of Fe atoms at FeN3-FeN3@graphene and found that FM state is 9.1 meV more stable than AFM state at HSE06 level, which agrees well with PBE+U calculations (main text, Page 2, Line 15-20). Furthermore, for the stepwise 2 and 4 CO molecules adsorption, the most stable spin alignment on adjacent Fe atoms is AFM state, agreeing with PBE+U calculations. In short, we have compared HSE06 and PBE+U results and argue that our main conclusion about the CO-induced spin transition on adjacent Fe atoms holds.

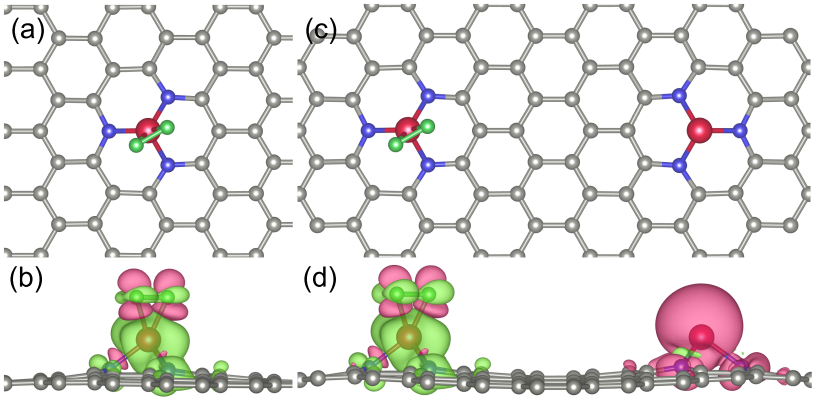

FIG. S2: Top view of the optimized structure of FeN_3 (a) and FeN_3-FeN_3 (c) after first O_2 molecule is adsorbed, (b) and (d) is the side view of net spin electron density of FeN_3 and FeN_3-FeN_3 at an isosurface value of 1×10^{-3} eÅ^{-3}.

Supplementary Note 1

We have also considered the O_2 molecules adsorption on the Fe sites of FeN_3-FeN_3 as shown in FIG. S2. O_2 molecule bonds to the Fe atom in side-on fashion and the O-O bond length is elongated by 0.20 Å whereas that is 0.18 Å in isolated FeN_3 active site. The calculated adsorption energy is 2.77 eV, 0.11 eV higher than that in FeN_3 system (2.66 eV). These indicate considerable adsorption enhancement if two active sites approach mutually, compared to single Fe site. Upon the O_2 adsorption, the geometrical structure of FeN_3-FeN_3 adjusted accordingly and all the geometrical symmetry disappeared. As shown in Table S2, the adsorbed O_2 alters not only the Fe-N bond length of the corresponding Fe site, but also that of neighbouring Fe site. Such associated structural transformation upon molecule adsorption cannot be observed in single FeN_3 system and it's indeed the indication of the existence of communicative effect between adjacent Fe sites of FeN_3-FeN_3@graphene.

More interestingly, one can see from FIG. S2(d), due to O_2 insertion, the spin moment of Fe atom is decreased to 2.74 μ_B, the net spin charge localized on Fe atom is reduced with part of them transferred to the adsorbed O_2. In contrast with CO adsorption, the magnetic interaction between O_2 and Fe center reverses the spin moment of Fe site it attached whereas CO reverses that of adjacent site. Although O_2 adsorption induces comparable structural transformation of Fe active center, it only leads to slight spin moment reduction on the nearby Fe site. As a result, the most energy-favorable spin ordering of FeN_3-FeN_3 shifts from ferromagnetic to ferrimagnetic with total spin moment of 1.12 μ_B. These two changes of the neighbouring Fe site signify that the interconnectedness of adjacent Fe centers exists and they communicate and interact indirectly via the graphene matrix, hinting that the mutual influence between the adjacent active sites need to be considered in analogous SAC frameworks. The spin transition upon the O_2 adsorption verifies that O_2 adsorption has, similarly to CO, led to 2D long-range ferrimagnetic orders on Fe sites, and the cooperative interaction between nearby Fe sites mediated by O_2 molecule can tailor the magnetic ordering of 2D material.

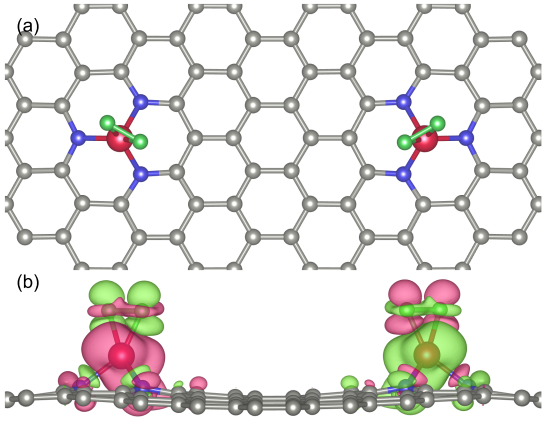

FIG. S3: (a) Top view of the optimized structure of FeN_3-FeN_3 after two O_2 molecules are adsorbed on the two individual Fe sites, (b) the side view of net spin electron density at an isosurface value of 1×10^{-3} eÅ^{-3}.

Supplementary Note 2

We further consider a second O_2 molecule adsorption on the neighbouring Fe site. The optimized structure after the second O_2 adsorption is shown in FIG. S3(a). The calculated O_2 binding energy is 2.59 eV, 0.18 eV weakening than the first O_2 adsorption. Upon the second O_2 adsorption, the Fe-N bond length readjusted slightly and the overall geometric symmetry (C_{2v}) reappeared summarized in Table S2. We further explore the response of spin state to such geometric adjustment. In the ground state after two O_2 molecules interact respectively with the Fe sites, the spin moment of corresponding Fe sites decreases from 3.39 to 2.76 μ_B whereas that of the neighbouring site with preadsorbed O_2 arises a little by 0.02 μ_B. The net spin charge is still mainly localized on the Fe sites and adsorbed O_2 molecules if seeing these two sites separately, much resembling to the O_2 adsorption in the single FeN_3 structure. However, if combined, one can see that the net spin moment of each individual Fe site is in the equal value (2.76 μ_B) but antiparallel, unambiguously indicating the 2D long-range antiferromagnetic (AFM) orders on Fe sites. This AFM spin ordering is completely different from the FM spin ordering when the Fe active sites are free from O_2 adsorption, although both of the structure are in the same C_{2v} symmetry. Meanwhile, one can see clearly in FIG. S3(b), the second adsorbed O_2 reverses not only the spin moment of Fe center it bonds, but also that of its nearby Fe site, which is also different from the second CO adsorption.

This synchronous spin transition of adjacent active sites again indicates inter-site cooperative communication arises when responding to the exterior electronic perturbation induced by CO or O_2 adsorption, if they approach to each other closely to deliver such perturbation effectively. More specifically, it further demonstrates that the communicative effect between two adjacent active sites can be tailored through external surface-molecular spin interaction and the desirable magnetic ordering on the Fe sites can be fine-tuned by controlling the O_2 adsorption.

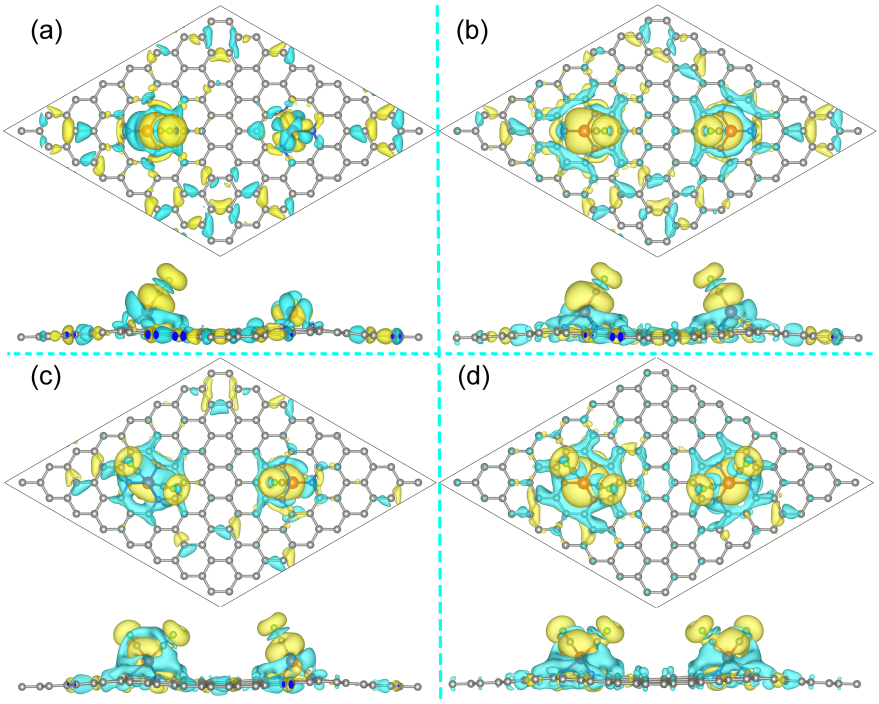

FIG. S4: (a) Top view and side view of charge density difference when one CO molecule adsorbed on the Fe atom of FeN_3-FeN_3@graphene. (b),(c) and (d) is for two, three and four CO molecules adsorbed on Fe atoms, respectively. The benchmark is the charge density when no CO molecule is adsorbed on Fe atoms. The isosurface value is 5×10^{-4} eÅ^{-3}. Yellow and blue bubbles represent charge accumulation and depletion, respectively.

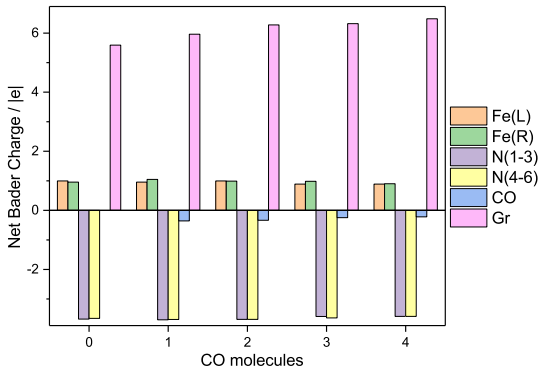

FIG. S5: Net bader charge of each section of the active sites, *i.e.* Fe atoms and three coordinated N atoms as a whole, and graphene matrix and CO, upon stepwise CO adsorption. The Fe and N atom are labeled as the Fig. S1 and the bader charge change of adsorbed CO is averaged.

Supplementary Note 3

In the Fig. S4, it indicates the inter-site charge redistribution of FeN_3-FeN_3@graphene framework upon CO adsorption, which is expected to cause the modification of charge-carrier concentration on graphene matrix hence the inter-site exchange coupling strength. Consequently, adjacent Fe atoms establish characteristic long-range spin ordering.

Clearly, once CO molecule is adsorbed on one Fe active sites, it leads to significant charge transfer in the corresponding site; Further, one can also see the adjoint charge transfer in its adjacent Fe site despite of no direct interaction from the injected CO molecule. Such communicative charge behaviors is the clear evidence of cooperative interaction between active sites. Additionally, the surface electron of graphene also experiences considerable depletion, which, as a bridge, interconnects the

adjacent sites, delivers the electronic perturbation induced by CO from site to site and further mediates effectively the indirect exchange coupling between two adjacent Fe active sites.

Bader charge analysis[19] in the Fig. S5 also indicates the charge transfer of the Fe active sites induced by CO adsorption. It reveals that the Fe atoms still positively charged and three N atoms negatively charged, which facilitates the charge redistribution on the Fe active sites and graphene matrix upon CO adsorption.

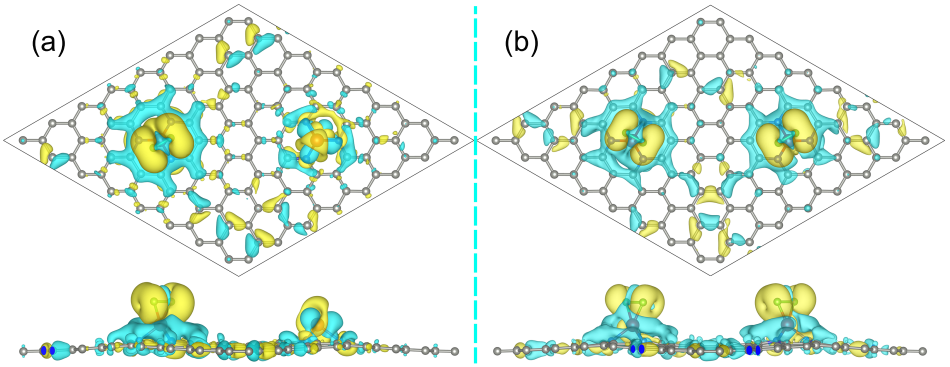

FIG. S6: Top view and side view of charge density difference when one (a) and two (b) O_2 molecule adsorbed on Fe active sites of FeN_3-FeN_3@graphene, respectively. The benchmark is the charge density when no O_2 molecule is adsorbed on Fe atoms. The isosurface value is 5×10^{-4} eÅ^{-3}. Yellow and blue bubbles represent charge accumulation and depletion, respectively.

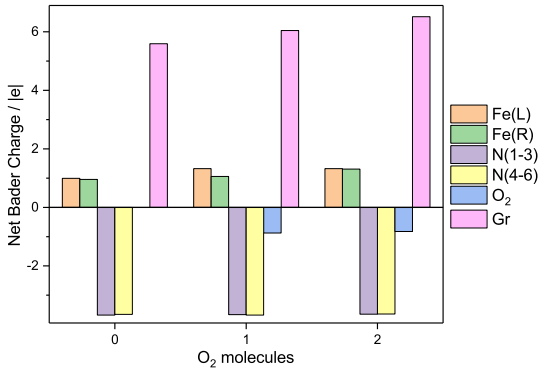

FIG. S7: Net bader charge of each section of the active sites, *i.e.* Fe atoms and three coordinated N atoms as a whole, and graphene matrix and O_2, upon stepwise O_2 adsorption. The Fe and N atom are labeled as the Fig. S1 and the bader charge change of adsorbed O_2 is averaged.

References

[1] Kresse, G. & Furthmüller, J. Efficiency of ab-initio total energy calculations for metals and semiconductors using a plane-wave basis set. *Comput. Mater. Sci.* **6**, 15 (1996).

[2] Kresse, G. & Furthmüller, J. Efficient iterative schemes for ab initio total-energy calculations using a plane-wave basis set. *Phys. Rev. B* **54**, 11169 (1996).

[3] Perdew, J. P., Burke, K. & Ernzerhof, M. Generalized gradient approximation made simple. *Phys. Rev. Lett.* **77**, 3865 (1996).

[4] Anisimov, V. I., Aryasetiawan, F. & Lichtenstein, A. First-principles calculations of the electronic structure and spectra of strongly correlated systems: the LSDA+U method. *J. Phys. Condens. Matter* **9**, 767 (1997).

[5] Dudarev, S., Botton, G., Savrasov, S., Humphreys, C. & Sutton, A. Electron-energy-loss spectra and the structural stability of nickel oxide: An LSDA+U study. *Phys. Rev. B* **57**, 1505 (1998).

[6] Ali, M. E., Sanyal, B. & Oppeneer, P. M. Electronic structure, spin-states, and spin-crossover reaction of heme-related Fe-porphyrins: a theoretical perspective. *J. Phys. Chem. B* **116**, 5849 (2012).

[7] Ali, M. E., Sanyal, B. & Oppeneer, P. M. Tuning the magnetic interaction between manganese porphyrins and ferromagnetic Co substrate through dedicated control of the adsorption. *J. Phys. Chem. C* **113**, 14381 (2009).

[8] Wäckerlin, C. *et al.* On-surface coordination chemistry of planar molecular spin systems: novel magnetochemical effects induced by axial ligands. *Chem. Sci.* **3**, 3154 (2012).

[9] Blöchl, P. E. Projector augmented-wave method. *Phys. Rev. B* **50**, 17953 (1994).

[10] Kresse, G. & Joubert, D. From ultrasoft pseudopotentials to the projector augmented-wave method. *Phys. Rev. B* **59**, 1758 (1999).

[11] Grimme, S. Semiempirical GGA-type density functional constructed with a long-range dispersion correction. *J. Comput. Chem.* **27**, 1787 (2006).

[12] Methfessel, M. & Paxton, A. High-precision sampling for Brillouin-zone integration in metals. *Phys. Rev. B* **40**, 3616 (1989).

[13] Bhandary, S. *et al.* Graphene as a reversible spin manipulator of molecular magnets. *Phys. Rev. Lett.* **107**, 257202 (2011).

[14] Ma, Y. *et al.* Evidence of the existence of magnetism in pristine VX_2 monolayers (X= S, Se) and their strain-induced tunable magnetic properties. *ACS Nano* **6**, 1695–1701 (2012).

[15] Anasori, B. *et al.* Control of electronic properties of 2D carbides (MXenes) by manipulating their transition metal layers. *Nanoscale Horiz.* **1**, 227–234 (2016).

[16] Jiao, Y., Sharpe, R., Lim, T., Niemantsverdriet, J. H. & Gracia, J. Photosystem II acts as a spin-controlled electron gate during oxygen formation and evolution. *J. Am. Chem. Soc.* **139**, 16604–16608 (2017).

[17] Miao, N., Xu, B., Zhu, L., Zhou, J. & Sun, Z. 2D intrinsic Ferromagnets from van der Waals Antiferromagnets. *J. Am. Chem. Soc.* **140**, 2417–2420 (2018).

[18] Zhang, J.-J. *et al.* Type-II multiferroic $Hf_2VC_2F_2$ MXene monolayer with high transition temperature. *J. Am. Chem. Soc.* **140**, 9768–9773 (2018).

[19] Henkelman, G., Arnaldsson, A. & Jónsson, H. A fast and robust algorithm for Bader decomposition of charge density. *Comput. Mater. Sci.* **36**, 354 (2006).